Process design, exergy, and economic assessment of a conceptual mobile autothermal methane pyrolysis unit for onsite hydrogen production

Meshach E. Tabat[1], Fredrick O. Omoarukhe[2], Fatih Güleç[3], Dare E. Adeniyi[4], Alivia Mukherjee[5], Patrick U. Okoye[6], Chukwuma C. Ogbaga[7,8], Emmanuel I. Epelle[9], Olugbenga Akande[10], Jude A. Okolie*[11]

[1]Process Engineering and Energy Technology, University of Applied Sciences Bremerhaven, Bremerhaven, Germany

[2]Department of Chemical Engineering, University of Ilorin, P. M. B. 1515, Ilorin, Nigeria.

[3]Low Carbon Energy and Resources Technologies Research Group, Faculty of Engineering, University of Nottingham, Nottingham, NG7 2RD, United Kingdom.

[4]Department of Mechanical Engineering, University of Ilorin, Nigeria

[5]Department of Mechanical Engineering, University of Alberta, Edmonton, Canada.

[6]Instituto de Energías Renovables (IER-UNAM), Privada Xochicalco s/n Col. Centro, Temixco, Morelos 62580, México

[7]Department of Biological Sciences, Nile University of Nigeria, Airport Road, Abuja, Nigeria

[8]Department of Microbiology and Biotechnology, Nile University of Nigeria, Airport Road, Abuja, Nigeria

[9]School of Computing, Engineering & Physical Sciences, University of the West of Scotland, PA1 2BE, Paisley, United Kingdom

[10] Department of Advanced Convergence, Handong Global University, 558 Handong-ro, Heunghae-eup, Buk-gu, Pohang, Gyeongsangbuk-do, 37554, Republic of Korea

[11]Gallogly College of Engineering, University of Oklahoma, Norman USA.

*Corresponding Author

Jude A. Okolie,

Assistant Professor,

Engineering Pathways, Gallogly College of Engineering,

University of Oklahoma, Norman, United States.

Jude.okolie@ou.edu

Abstract

The present study proposes a conceptual mobile autothermal methane pyrolysis unit for onsite hydrogen production. Considering the shortage of hydrogen pipeline infrastructure between production plants and fuelling stations in most places where hydrogen is required, it is imperative to create alternative hydrogen production means. The design combines a catalytic plasma methane pyrolysis unit with a steam char gasification setup, combustion, and biomethanation unit for hydrogen production. The reactor design includes a Ni - Br in a bubble column acting as a catalyst. Energy and exergy calculations followed by a comprehensive economic analysis were appraised to evaluate the efficiency and performance of the integrated process. The levelized cost of hydrogen (LCOH) from the conceptual design ranged from 1.3 – 1.47 U.S.$/kg. While the proposed design's net present value (NPV) was in the range of 3.76 – 4.35 M.U.S.$. Factors such as equipment purchase cost (EPC) and feedstock cost significantly influenced the NPV and LCOH. In addition, a positive NPV and lower LCOH outline the proposed design's profitability. Finally, an optimized methane conversion of 76.8% was obtained from the study.

Keywords: Hydrogen; Methane pyrolysis; Simulation; Techno-economic analysis; Life-cycle assessment.

Abbreviations

AEA Aspen Economic analyzer

CapEx Capital expenditure

CCS Carbon capture and storage

EPC Equipment purchase cost

LCOH Levelized cost of hydrogen

NPV Net present value

OpEx Operating expenses

PFR Plug flow reactor

ROI Return on investment

SMR Steam methane reforming

TEA Techno-economic analysis

Graphical Abstract

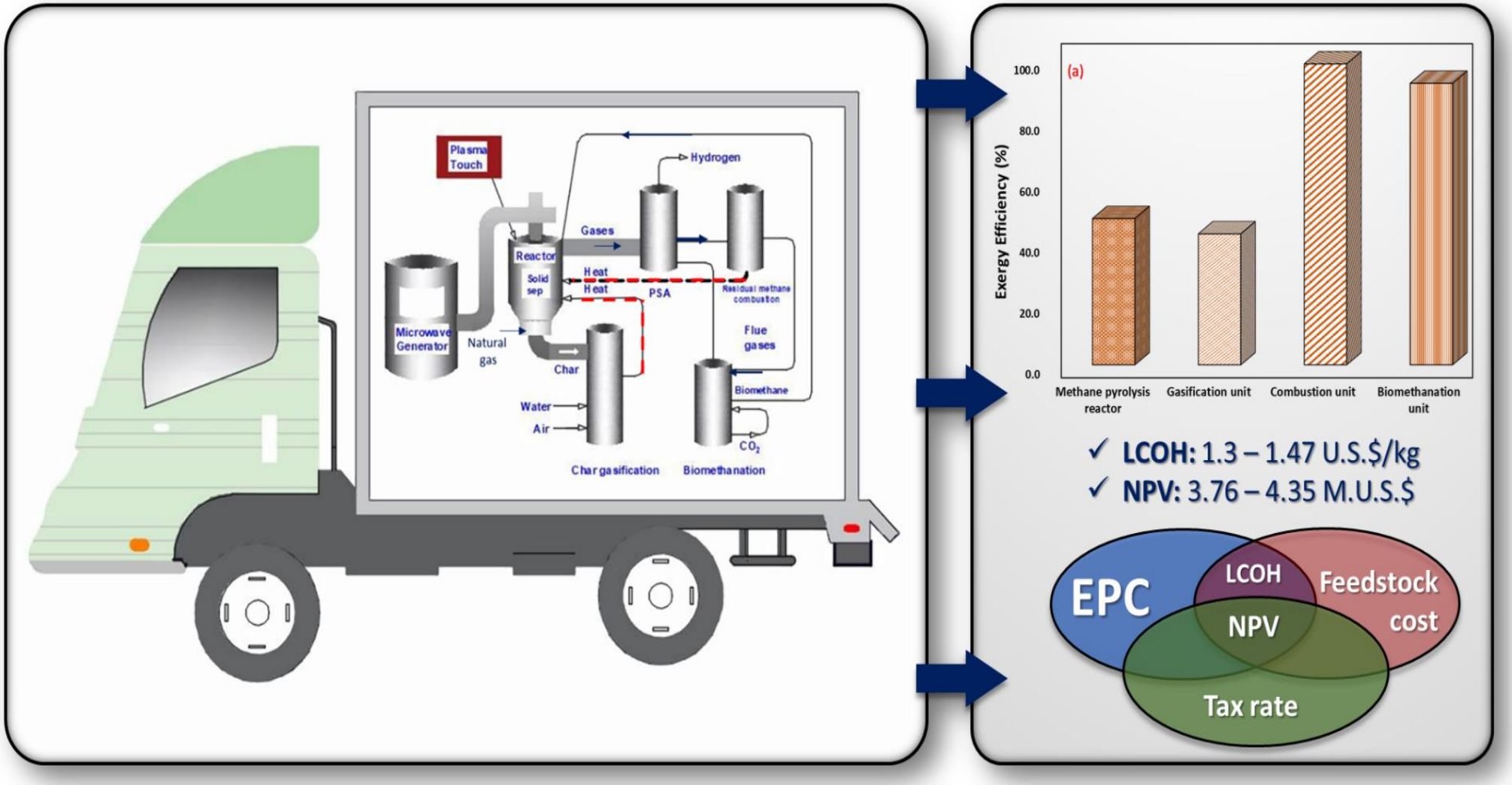

1. Introduction

The increasing world population, industrialization, and urbanization ~~re~~ are some of the reasons for the skyrocketing energy demand [1]. Although petroleum-based resources are used to address the elevating energy demand, their utilization is accompanied by environmental pollution issues, price fluctuation, and depleting petroleum reserves. As a result, the interest in alternative energy sources that are cheap and sustainable has increased over the years. Hydrogen is highly regarded as a versatile energy carrier that can complement fossil fuels and promote a net-zero economy.

The interest in hydrogen is due to its diverse industrial applications and pollution-free characteristics. Hydrogen can be used in heavy oil refining, fuel cells, platform chemicals synthesis, pharmaceuticals, and metallurgical industries. Moreover, hydrogen releases water during combustion and has a very high calorific value (141.9 kJ/g) when compared to gasoline (54 kJ/g) [2]. Most countries, businesses, and organizations envision hydrogen playing a major role in the energy transition. Using clean hydrogen as a substitute for fossil fuels could play a critical role in the decarbonization of future energy systems and the transition to a CO_2 neutrality-based economy [3]. However, it should be noted that most of the hydrogen produced today is from the steam methane reforming (SMR) of petroleum resources, most commonly natural gas, a process that releases about 900 Mt CO_2–eq per year (equivalent to 2% of the worldwide CO_2 emissions) [4]. Therefore, it is imperative to produce hydrogen from pathways that minimize greenhouse gas emissions and net production costs. However, some companies have started producing commercial-scale blue hydrogen using SMR with carbon capture and storage (CCS). The challenges of long-term hydrogen storage and transportation remain unsolved. Currently, onsite hydrogen production is mainly based on water splitting through electrolysis, which is expensive.

Methane pyrolysis is a promising pathway for hydrogen production from natural gas. The reaction involves the decomposition of methane into hydrogen and solid carbon in the absence of water and oxygen at high temperatures, as shown in reaction 1 [1]. Compared to other hydrogen production pathways, methane pyrolysis does not produce CO_2. Instead, it produces solid carbon, which has ample industrial applications [5]. Methane pyrolysis-derived carbon black could be used in synthesizing carbon nanotubes, activated carbon, carbon fibres, and graphene or as heterogeneous catalyst support [5].

Moreover, the logistics involved in transporting solid carbon are easier than CO_2. A recent study critically discussed the opportunities and progress of methane pyrolysis for hydrogen production [6]. The authors noted that methane pyrolysis has the potential to act as a bridge between petroleum resources to renewable energy systems [6].

$$CH_4 \leftrightarrows C_{(s)} + 2H_{2(g)} \quad \Delta H = 74.8 \text{ KJ/mol} \qquad \text{(Reaction 1)}$$

Overall, the decomposition of methane to produce carbon black and hydrogen is an endothermic process requiring considerable energy. Depending on the energy input of the process, two main methane pyrolysis pathways are often used: thermal and plasma processes [7]. Thermal processes require a high temperature of more than 1000^{o}C, thereby increasing the overall processing cost [6]. Although, catalysts are often used to elevate the reaction rate, improve the methane conversion and lower the reaction temperature [8].

Compared to the thermal processes, plasma pyrolysis improved methane conversion and high carbon and hydrogen yield [9]. Furthermore, the non-thermal plasma process proceeds at a lower temperature range [8]. Non-thermal Pyrolysis uses plasma sources such as microwaves, dielectric barrier discharge, gliding arcs, or electron beams to split methane into carbon black and hydrogen at higher efficiency [10]. The high-energy electrons produced by the non-thermal processes enhance the chemical processes leading to hydrocarbon decomposition. Thus, the

process is characterized by high selectivity and reactivity, low energy consumption at lower temperatures, and atmospheric pressure [11].

Much research has been carried out in the field of plasma methane pyrolysis for the decarbonization of natural gas [10,12,13]. Most of the studies pay attention to the chemical kinetics of plasma pyrolysis [14] or the evaluation of the reaction mechanism and equilibrium composition [12], or the development of different pyrolysis-modified reactors to overcome the limitations of sizeable external energy supply resulting from increasing temperature demand [15–17]. To the best of the authors' knowledge, studies on the design of a mobile autothermal plasma methane pyrolysis unit have not been reported. Considering the shortage of hydrogen pipeline infrastructure between production plants and fuelling stations in most places where hydrogen is required, it is imperative to create alternative hydrogen production means. The mobile methane pyrolysis unit helps to eliminate the challenges of hydrogen storage and transportation by producing hydrogen onsite in the desired location. To fulfil the knowledge gaps, this study presents the design and stochastic economic evaluation of an autothermal plasma methane pyrolysis unit for onsite hydrogen production. The study aims to demonstrate the economic competitiveness of the proposed process. Furthermore, Ni - Br in a bubble column acting as a catalyst will be incorporated as part of the methane pyrolysis reactor. It is anticipated that the proposed technology could help advance economically feasible hydrogen production from natural gas.

2. Relevant literature and study novelty

Plasma methane pyrolysis has received significant attention, and the results are documented in several publications. Kerscher et al.[1] performed a comprehensive techno-economic analysis (TEA) and carbon footprint assessment of electron beam plasma methane pyrolysis for hydrogen production. The LCOH from the technology ranged between 2.72 U.S.$/kg H_2 and

5.34 U.S.$/kg H_2. Furthermore, the process led to a reduction in greenhouse gas emissions compared to other hydrogen production pathways. Akande and Lee.[11] developed an experimental setup for a non-catalytic plasma methane steam reforming process [11]. A hydrogen production rate of 2247 g(H_2)/h was obtained from the process [11].

Recently, a swirl-induced point-plane discharge reactor was developed and tested for the direct conversion of methane to hydrogen and carbon black [18]. Hydrogen yield and selectivity of 16% and 84%, respectively, were reported. Although, other hydrocarbons, such as ethane and acetylene, were also detected as part of the products.

Among different plasma sources, microwave plasma is advantageous in terms of its ability to operate without an electrode and rapid time of response from electricity to torch [11]. Some researchers studied the methane conversion mechanism for three different plasma sources, including microwave plasma, gliding arc plasmatron, and dielectric barrier discharge [19]. The authors noted that thermal conversion plays a significant role in the hydrogen formation mechanism while vibrational-translational non-equilibrium has a minimal role.

Existing research contributions related to methane pyrolysis for hydrogen production can be categorized into the optimization of process parameters during microwave plasma pyrolysis or the evaluation of the reaction mechanism or catalyst development. The main catalysts for methane pyrolysis include nickel-, iron-, doped noble metal- and carbon-based catalysts. Ni-based catalysts are preferred due to their low cost and promising hydrogen selectivity [6]. Several authors have reported the use of Ni-based materials for catalysis during methane pyrolysis. Parmar et al. developed a nickel-based catalyst with an optimal composition of 60%Ni-5%Cu-5%Zn/Al_2O_3 and used the catalyst to achieve a 90% methane conversion under fluidized bed bubbling conditions [20]. Another study reported an increase in methane conversion from 28 – 49% with Ni/MgO catalysts under low-temperature Pyrolysis at (600 °C)

[21]. Recently, some researchers proposed a multi-stage bubble column reactor containing molten Ni-Bi alloy, zirconia, and molten NaBr as catalysts for efficient hydrogen production from methane pyrolysis [22]. Considering the previous studies in the literature already discussed, there are three significant knowledge gaps this study attempts to address:

- High-fidelity process simulation and design of an autothermal mobile microwave plasma pyrolysis unit that is moveable and can produce hydrogen from natural gas.
- Comprehensive energy and exergy analysis of each process stream.
- Detailed techno-economic and sensitivity analysis of the mobile unit to evaluate the economic impact.

The results will be helpful for the development of mobile biomass pyrolysis systems, especially in North America.

3. Methodology

3.1 Process Design and Description

. Detailed information on the process flow diagram simulated in Aspen plus can be found in figure 1 while Figure 2 illustrates the flow diagram of the mobile unit. The process consists of a microwave plasma methane pyrolysis reactor unit, gas-solid separation unit, char gasification and biomethanation unit, and product separation and purification unit.

The process was simulated in Aspen Plus V 9.0 (Aspen Tech, Bedford, USA); the simulation package was also used to evaluate the mass and energy balances. The Aspen package contains an inbuilt physical properties database where Peng-Robinson was used as the base method for robust thermodynamic calculation and implementation of the hydrocarbon system.

Pure methane feed at ambient temperature and pressure is compressed isentropically to a reaction pressure of 2.5 bar and preheated to about 400 ^{o}C. After which the reactor is preheated to a temperature of about 600 ^{O}C before the methane enters. Preheating the reactor to 600 ^{O}C with air plasma is more beneficial than preheating methane alone. Preheating methane can be done by passing it through the refractory of the preheated reactor in a reverse direction since studies have shown that preheating methane to 400 ^{o}C enhances conversion [11]. Typically, methane is supplied in a compressed gas cylinder above 10 bar; a pressure reducer can decrease the pressure to 2.5 bar. A compressor is needed for the recycling of methane. The methane compression was performed by incorporating a portable and moveable natural gas compressor unit at the feed inlet station. The gas is compressed mechanically, in stages, to different pressurization amounts to meet the desired delivery level. The compressor could be powered by a portable natural gas tank attached to the unit or a buffer battery.

The methane pyrolysis unit was modelled independently with two different kinds of reactors: the RGibbs reactor and the plug flow reactor (PFR). The results from PFR were also compared with the RGibbs reactor and experimental data from the literature. The RGibbs block was selected because of its ability to accurately estimate the phase equilibrium and chemical equilibrium of multiphase systems. Furthermore, some researchers have used the RGibbs reactor to calculate the phase equilibrium reaction for thermochemical processes [23–27]. The PFR was implemented because of its ability to perform equipment sizing, define the underlying pyrolysis reactions, and provide catalyst information. The PFR was also able to capture the complexities related to the liquid metal system. Details of the plug flow reactor design implemented in Aspen plus and the underlying assumptions are discussed in section 3.2.

It should be mentioned that the high reaction temperature is due to the reaction's endothermicity and strong C-H bonding. Therefore, increased temperature is required to split the C-H bond

and improve hydrogen yield. The methane pyrolysis reaction products include gaseous products such as hydrogen, unreacted methane, and solid carbon black.

The solid carbon black was removed from the reaction products in the gas-solid separation unit. The unit was modelled using the cyclone (B6) in Aspen Plus. The separation was performed based on the fraction of vapour-to-vapour outlet and the fraction of solid-to-solid outlet with values 1 and 0.999, respectively. The solid, purely carbon graphite, exited the unit by gravity at the bottom of the reactor as CHAR, while the gases exited the unit at the top for further separation. Since the conceptual design is an autothermal process, the reactor and feed preheater are expected to use the heat generated in situ. Therefore, a carbon gasification unit was added. This unit was used to generate energy for the overall autothermal process through steam gasification of the produced char. The carbon gasification unit was modelled with the RGibbs reactor.

H_2 was recovered from the product gas with a palladium membrane. The H_2 separator was modeled with the design specification of the HYSEP Technology model (HYSEP Modul Type 108, ECN, palladium membrane filter) [28]. This is the smallest HYSEP membrane module with a total area of 0.04 m^2. It is advantageous because of the lower capital and operating cost, size flexibility, and higher hydrogen separation efficiency [28]. Aspen plus modeling of HYSEP 108 was performed with a ready-made FORTRAN user model incorporated in Aspen PLUS. The membrane specifications were defined with an excel sheet integrated into Aspen Plus. The model's details have been meticulously described elsewhere [29]. Moreover, a 98% capture efficiency is assumed, typical of the HYSEP 108 membrane separator [28].

The carbon from the gas-solid separator unit was sent to the gasifier alongside steam. It compressed air as feed in the ratio (1:1:5). The high amount of air used in the simulation is due to the low fraction of oxygen in the air (i.e., 21%). The carbon was completely combusted,

releasing a significant amount of energy and by-products, including CH_4, H_2, CO, CO_2, H_2O, and N_2. The gaseous products were cooled with a heat exchanger (B12) and cooling tower (CTOWER) to strip the gas from the liquid present. A water gas shift reactor (WGS) was used to convert the produced CO into hydrogen.

The CO was stripped from the other gases with a membrane separator (B24) and forwarded to the WGS reactor alongside steam (generated in the heat exchanger B12). The water gas shift reactor is a system that converts the produced CO into CO_2 and H_2, as shown in reaction 2.

$$CO + H_2O \leftrightarrow CO_2 + H_2 \quad \text{(Reaction 2)}$$

This reaction was modelled using the equilibrium reactor (B27) to achieve system's phase and chemical equilibrium. The CO gas was completely converted to CO_2 and H_2, after which the products were sent to a cooling tower (B31) to strip water from the gas. These gases are then combined with other gases from various units for further separation.

The gases exiting the top of the gas-solid separator were cooled to 650 ^oC and separated by a membrane filter in the CH_4 separation unit. The technology proposed for the CH_4 separation unit is a zeolite-based membrane filter, assuming that about 98% of the methane is trapped in the filter [30]. The membrane filter was simulated in Aspen Plus with the same procedure as the H_2 separation membrane. The retrieved unreacted and produced CH_4 gas from the carbon gasification unit were combusted with compressed air (methane to oxygen ratio of 1:2) to produce water vapour and CO_2, as shown in reaction 3.

$$CH_4 + 2O_2 \rightarrow CO_2 + 2H_2O \quad \text{(Reaction 3)}$$

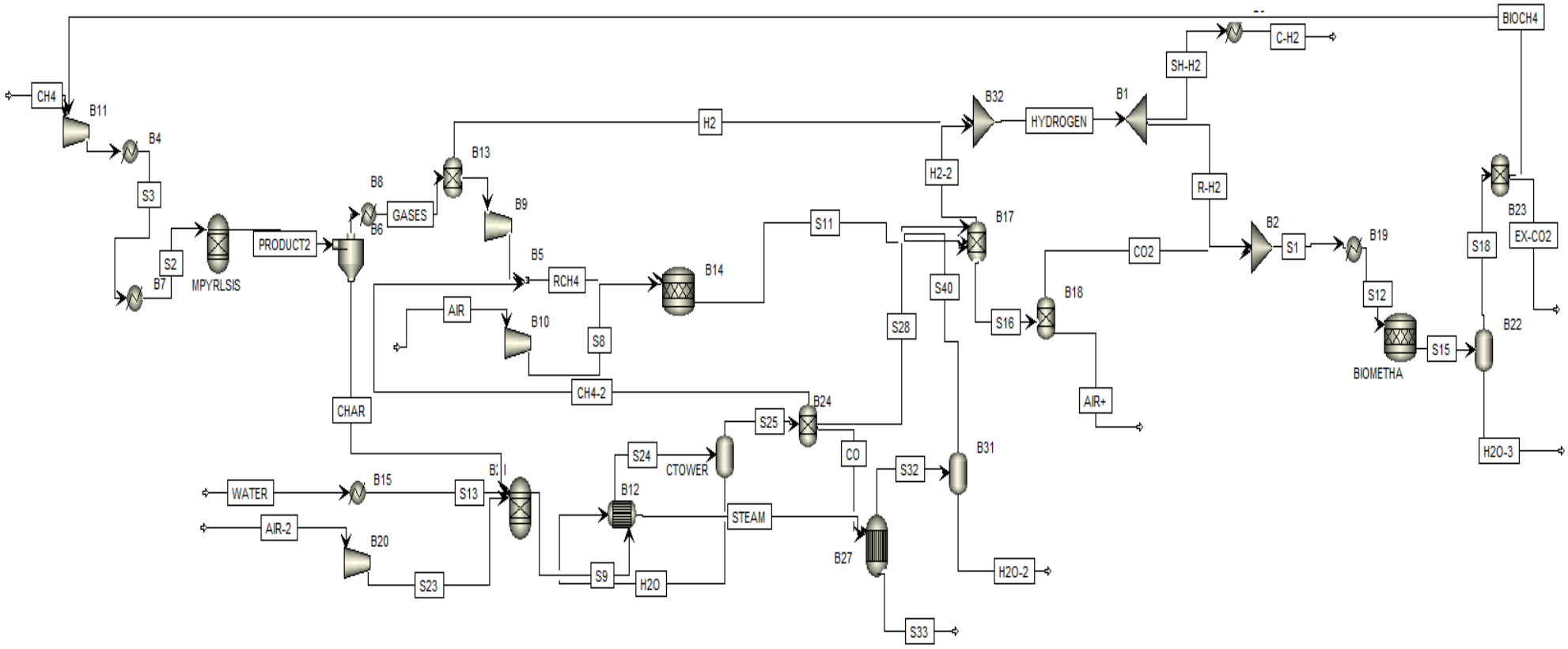

191

192 Figure 1: Process flow diagram of the conceptual design of a microwave plasma autothermal mobile methane pyrolysis unit for hydrogen
193 production.

194

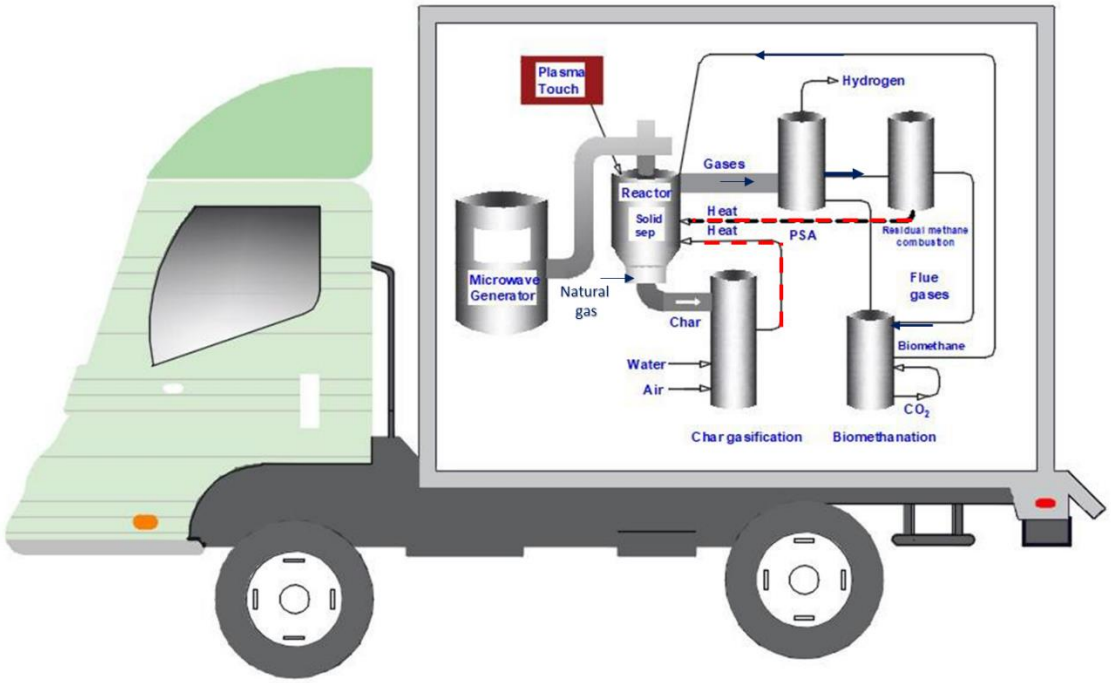

Figure 2: Schematic representation of the conceptual design of a microwave plasma autothermal mobile methane pyrolysis unit for hydrogen production.

The reaction is highly exothermic; thus, the energy released from this unit and the carbon gasification unit is sufficient to meet the energy requirement for methane pyrolysis and other heating units.

The products from the methane combustion unit are sent into a membrane separator (B17), combining the gases from the carbon gasification unit and the water gas shift unit to strip off the hydrogen produced (from these three-unit processes) with a 99.9% recovery rate. The hydrogen recovered is then combined with the hydrogen produced from the methane pyrolysis unit to yield 32.91% hydrogen from the overall system. An additional biomethanation unit was added for efficient product recovery and utilization.

The biomethane production unit is added as an innovative way of utilizing the produced CO_2 to obtain biomethane. Therefore, 30% of the produced hydrogen was used for the biomethanation process according to the reaction shown in reaction 4.

$$CO_2 + 4H_2 \rightarrow CH_4 + 2H_2O \qquad \text{(Reaction 4)}$$

The above reaction was modelled with a stoichiometric reactor (RStoic- BIOMETHA) at a mesophilic temperature of 70 ^{O}C and pressure of 5 bar. The products from the reactor, which comprised methane, water, and unreacted CO_2, were cooled in a flash drum (B22) to strip the gases from the water. The gases (mainly biomethane and unreacted CO_2) were then sent to a membrane separator modelled as SEP (B23) to completely separate the biomethane gas from the unreacted CO_2. Furthermore, the produced biomethane is recycled as feed.

3.2 Microwave-based plasma torch and reactor concept.

Schematics of the conceptual reactor design are illustrated in Figure 3a. The mobile microwave-based plasma torch reactor is designed to process 100 kg/hr of methane, equivalent to 2.65 tons/day. The reactor and other units were positioned in a manner that makes it convenient to be towed behind existing work vehicles and access remote sites through existing

roads. This places a lot of limitations on the volume, a 1 – ton U.S truck could take between 5-6 tons towing loads depending on the model and manufacturer [31]. Therefore, a reactor length of 1.4 m and external diameter of 0.5m was selected. The length limitations and selection are based on the standard road size in the United States

Moreover, most trailers have size constraints within the following limitations: 2.6 m wide, 4.3 m high, and 12.2 m long [32]. Reactor sizing was modelled with a PFR with all assumptions, reaction, and kinetic parameters listed in Table 1. It should be mentioned that the simulation of plasma pyrolysis reactors is highly complex due to the steep gradients and the number of temporal and spatial ranges of the variables involved. However, the PFR provides a decent representation of the reactor for preliminary economic evaluation.

Table 1: Assumptions in Aspen PLUS reactor modelling.

Assumptions	**Values**
Reaction Parameters [33]	Equation: $CH_4 \rightarrow 2H_{2(g)} + C_{(s)}$ Apparent activation energy: 277 kJ/mol
Feed Properties	Pressure: 1atm. Temperature: 25ºC. Flowrate: 100 kg/hr.
Fluid Package	Peng Robinson.
Reactor information	Aspen plus modelling block: Plug Flow Capacity: 100 kg/hr Length: 1.4 m External diameter: 0.5 m

The proposed non-electrode microwave plasma torch system is presented in figure 3b. The system is similar to the design proposed by Akande and Lee.[11] with modifications in reactor design and the use of a catalyst. Details of the system are described in figure 3a-c. The system consists of a microwave generator (915 MHz and power capacity up to 0.1 MW), a WR430 rectangular waveguide, optical emission spectroscopy system, a power generator for the microwave generation unit, a forward and reverse power monitor and flow control devices. It should be mentioned that the maximum power of a commercially available 2.45 GHz magnetron is 15 kW (0.015 MW), therefore a 915 MHz Microwave generator with a capacity of up to 100 kW (0.1 MW) was implemented.

The gas supply in the reactor is consistently monitored and controlled with a digital mass flow meter. It should be mentioned that the absorbed microwave power, which indicates the amount of microwave power provided to the discharge area, was determined from the numerical difference between the reflected and incident power. For plasma generation, a capacitively coupled system is implemented in connecting the microwave generator to the reactor.

The reactor is designed as a multi-layered liquid metal bubble column. Pure methane flows into the reactor from the bottom while the pyrolysis products, excluding solid carbon, are removed from the top section. A molten metal comprising of Ni-Br in a bubble column is used to catalyze the pyrolysis reaction, while the molten salt helps to separate carbon. It should be noted that the Ni-Br molten metal catalyst was selected based on experimental results from previous studies [34].

Catalytic methane pyrolysis leads to the formation of solid carbon that is often entrained in the gas stream exiting the reactor. Therefore, it is possible to separate the solid carbon from the gas stream through conventional processes such as cyclones or electrostatic separators. However, the use of molten salt is more economically feasible. The presence of a supporting layer of

molten salt on the surface of the metal often led to the aggregation and accumulation of insoluble carbon on the salt surface. Additionally, maintaining a layer of molten salt on a catalytic molten metal ensures that a liquid heat transfer fluid is efficiently circulated once the carbonaceous solid leaves the reactor [35]. The carbon floats on top of the molten salt layer that resides on top of the molten metal since the difference in density between various solids determine their placement in the reactor. It should be mentioned that the efficient and controlled transportation of liquid metal throughout the reactor vessel still poses challenges related to engineering design and construction materials. To address the challenges, some authors have employed bubble-lift pumps to improve the molten metal circulation [36]. The use of electromagnetic pumps for continuous molten metal streams has also been proposed in previous studies [36]. However, the proposed design faces challenges related to the high density of Ni-Bi, especially for bubble-lift pumps; therefore, extra layers of molten $MgCl_2$-NaCl salt above the Ni-Bi media have been suggested by another study [35]. The molten salt layer helps in the continuous removal of the produced carbon from the molten metal reactor, even at low-concentration slurry. A similar approach was adopted in the conceptual design proposed in this study. The molten salt comprises Mg-Cl_2 salt that is insoluble in carbon; that way, the precipitation of the materials on the heat exchanger walls could be avoided [37].

Aspen Plus simulation results (methane conversion efficiency) for both RGibbs and Plug flow reactor are compared with experimental values from the literature [38,39]. Since the conceptual design is novel, there are hardly any studies with similar operating conditions or reactor configurations. However, comparing the results provides a valid basis for preliminary economic appraisal. As shown in figure 4, the optimum methane conversion from the PFR and RGibbs reactor appears similar, with a 2% deviation. Also, the methane conversion reported herein is similar to those reported in the literature for plasma steam methane reforming [11] and microwave plasma source-enhanced pyrolysis [39].

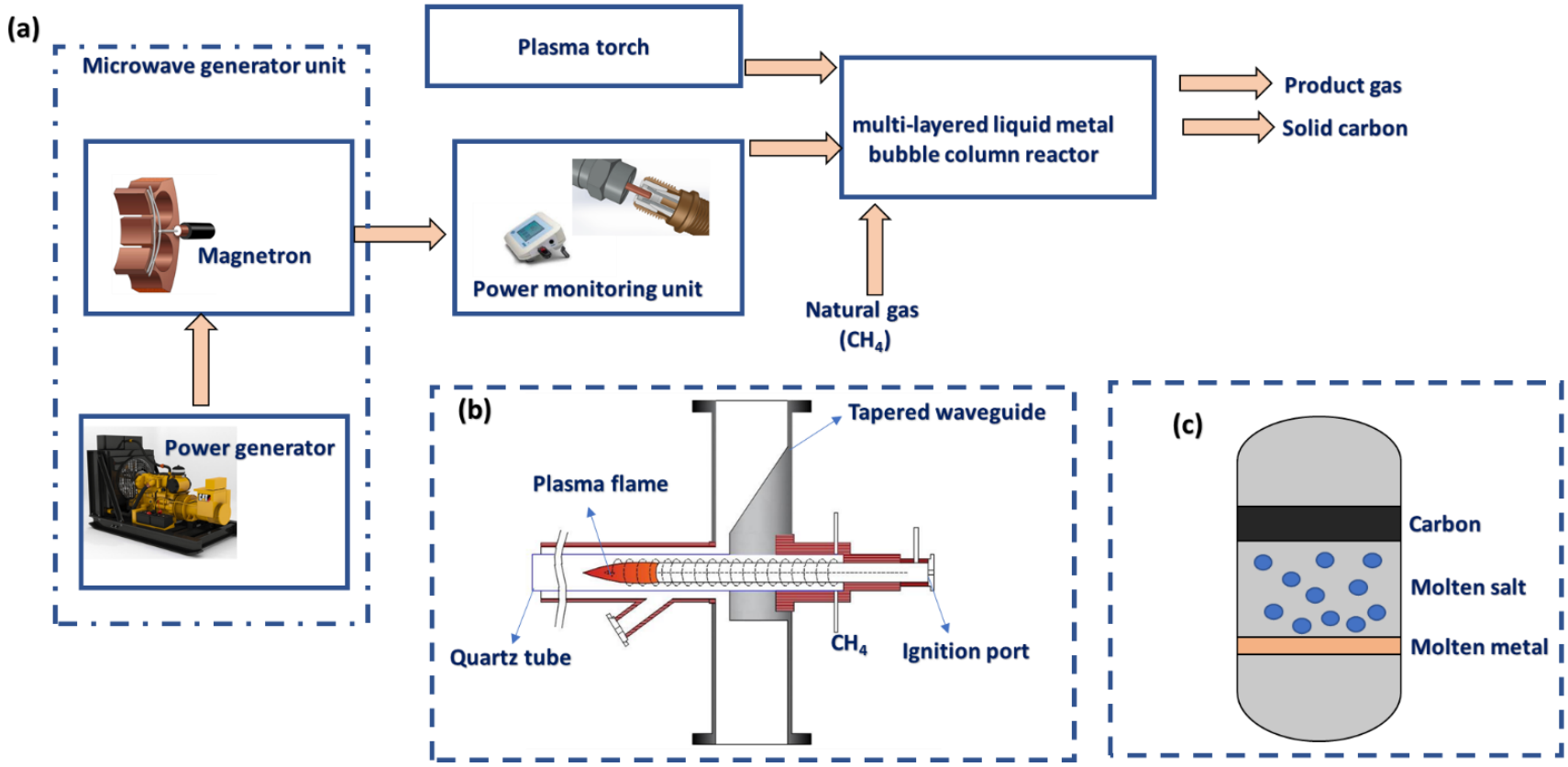

Figure 3: (a) Flow diagram of the conceptualized integrated microwave-based plasma torch with a multi-layered liquid metal bubble column reactor. (b) Overview of the proposed microwave plasma torch (c) Overview of the multi-layered liquid metal bubble column reactor.

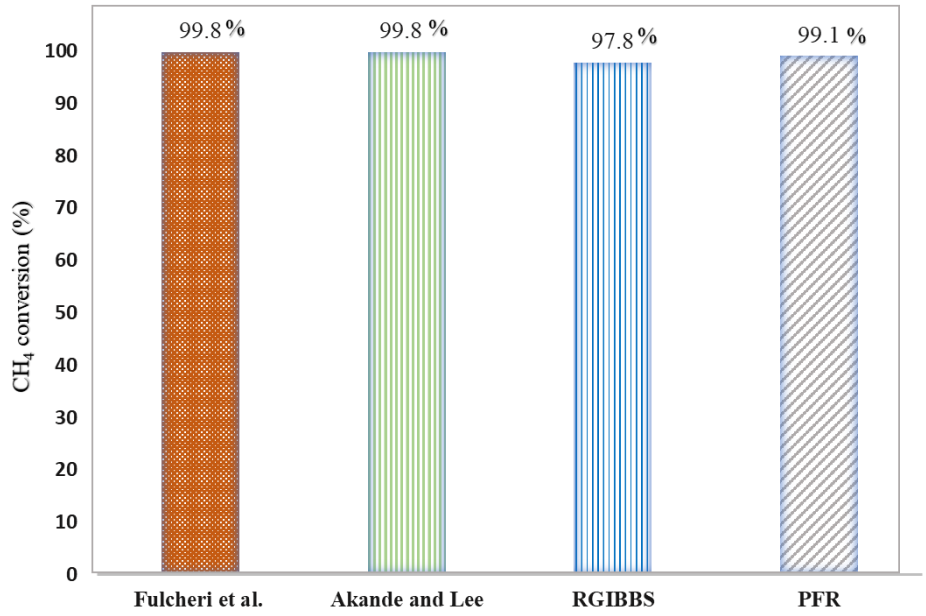

Figure 4: Comparison of the maximum CH_4 yield from the PFR and RGibbs reactor with literature values. Note that the operating conditions and reactor configurations are different.

3.3 Economic assessment

The capital investment cost of the proposed mobile autothermal plasma methane pyrolysis unit varies for different locations. Therefore, the techno-economic analysis (TEA) was performed assuming that the unit is in North America. The equipment purchase cost (EPC) was determined from a combination of the Aspen Economic analyzer (AEA), literature search [41] and CAPCOST software by Turton et al. [40]. Moreover, the AEA was also used to appraise the plant-wide cost of heat exchangers. In some cases where the equipment may have an out-of-range capacity, a literature search is combined with the scale factor rule to evaluate the EPC (equation 1).

$$\frac{C_a}{C_b} = \left(\frac{A_a}{A_b}\right)^n \quad (1)$$

Where C_a represents the cost of the new plant with capacity A_a. C_b is the cost of the initial plant with capacity A_b. n is the scale factor, which is assumed to be 0.8 for the proposed design [41].

All the estimated costs were scaled up to 2022 by applying the chemical engineering plant cost index.

The capital expenditure (CapEx) was evaluated as a fraction of the EPC. Also, the operating expenditure (OpEx) was appraised based on the labour cost, production capacity, and feedstock used. OpEx comprises all costs of production, such as variable (direct) costs, i.e., raw materials or utilities, and fixed (indirect) costs, including labour and maintenance costs. In contrast, CapEx comprises investment incurred for the plant construction, also known as inside battery limits, and investment for connecting the plant to the outside world; these include the roads, railroads, or general service facilities like power plants (outside battery limits) [42]. The inside battery limit comprises all the cost items required to build the plant's core production facilities, and everything required to build the plant facilities, and everything directly needed for production. A detailed description of the CapEx and OpEx computations has been summarized in the supplementary information (Table S1 and S2).

Equipment repairs and maintenance are part of the fixed and variable expenses based on yearly usage. Generally, equipment repairs, and maintenance cost often increases over time. Data for long-term repairs and maintenance is unavailable for most proposed design equipment. Therefore, the cost was assumed as a fixed percentage of a straight-line depreciation method over the lifetime of each piece of process equipment [43]. The frequency of maintenance is determined based on a 760 days per year maintenance while the plant will be in operation for 8000 hr/yr. The cost incurred during the portable system relocation depends on several factors, such as plant capacity, relocation distance, and labour cost. The cost of relocation is assumed to be a part of the yearly operating cost.

Economic indicators such as net present value (NPV) and return on investment (ROI) are used to measure the economic performance of the conceptual design. NPV is the sum of the present

values of all cash flow, including the initial investment [44]. In contrast, ROI directly measures the amount of return on the proposed conceptual design against the investment cost. The NPV and ROI are estimated from equations 2 and 3, respectively.

$$NPV = -TCI + \sum_{t=1}^{20} \frac{Net\ cash\ flows}{(1+i)^t} \quad (2)$$

$$ROI = \frac{Annual\ income}{Capital\ investment}\ x\ 100\% \quad (3)$$

The Levelized cost of hydrogen produced (LCOH) is used as an economic metric to quantify the economic feasibility of the conceptual design. It accounts for the capital and operating costs incurred during hydrogen production. It is a critical metric that enables the comparisons between different hydrogen production routes. LCOH considers the initial investment due to plant construction and the management costs over the entire lifetime [45]. It should be mentioned that the LCOH varies significantly with the size of the plant, the sources of energy, and the plant configuration.

The LCOH can be estimated from equation 4.

$$LCOH = \frac{Total\ production\ cost}{Annual\ hydrogen\ production} \quad (4)$$

3.4 Exergy analysis

The exergy of a system indicates the amount of useful work it can perform upon the realization of thermodynamic equilibrium with the environment. It shows the overall totality of the physical, chemical, potential, and kinetic exergy [47]. The total exergy of a system shows the direction or flow of work based on the second law of thermodynamics. Exergy analysis is helpful for the comparative evaluation of systems and components in making a well-informed design decision. Compared to energy analysis, exergy analysis shows the causes, locations, and

quantitative description of the system inefficiencies and integrates irreversibility in the thermodynamic assessment [48].

For a particular system, the exergy balance includes the exergy of input and output, as indicated in equation 5.

$$\sum \dot{E}_{loss} = \sum \dot{E_{input}} - \sum \dot{E_{output}} \quad \textbf{(5)}$$

Where $\sum \dot{E_{input}}$ and $\sum \dot{E_{input}}$ represents the overall exergy of the input and output stream in MJ/kg, respectively. $\dot{E}_{loss}$ is the exergy loss in the system in MJ/kg. Considering that the kinetic and potential energy of the system could be negligible, the exergy of a certain component stream, i ($\dot{E}_{stream,i}$) in the system would include both the chemical ($\dot{E}_{ch,i}$) and physical exergy ($\dot{E}_{ph,i}$ **)**.

$$\dot{E}_{stream,i} = \dot{E}_{ch,i} + \boldsymbol{\dot{E}_{ph,i}} \quad (6)$$

The overall exergy efficiency is estimated from the expressions in equation 7 [49]:

$$n_{exergy} = \frac{\dot{E}_{output}}{\dot{E}_{input}} x\ 100 \quad (7)$$

where $\dot{n}_{SJF}$ and $L\dot{H}V_{syngas}$ represent the mole flow rate and lower heating values of hydrogen.

Although the chemical exergy of several compounds is available in the literature, it is very difficult to define the chemical exergy of solid chars and gaseous and liquid product streams obtained during pyrolysis [50]. There are several correlations for estimating the chemical exergy of solid and liquid fuel components. In the present study, the chemical exergy proposed by Kaushik and Singh [51] was used to estimate the exergy of solid char with the assumption that the char contains negligible ash and sulphur contents (equation 8).

$$\dot{E}_{ch,solid} = (LHV_{db} + \lambda x_m).\beta_{db} + 9417x\ \dot{x}_{s,db} \quad (8)$$

Where LHV_{db}, $\lambda, and\ x_m$ represent the lower heating value of the solid on a dry basis, latent heat of vaporization of water at room temperature, and mass fraction of moisture, respectively. β_{db} and $\dot{x}_{s,db}$ represent the ratio of the specific chemical exergy of the compound to the LHV and mass fraction of sulphur, respectively.

The exergy of the liquid phase mixture ($\dot{E}_{ch,liquid}$) is calculated from equation 9 [50,51].

$$\dot{E}_{ch,liquid} = \frac{\boldsymbol{M_{liquid,i}}}{\mathbf{100}} \dot{E}_{ch,water} + \frac{\mathbf{100} - \boldsymbol{M_{liquid,i}}}{\mathbf{100}} \dot{E}_{ch,og,i} \quad (9)$$

$\boldsymbol{M_{liquid,i}}$ is the water content mass fraction in a specific flow stream and $\dot{E}_{ch,og,i}$ is the chemical exergy of the representative organic compound in phase i expressed in MJ/kg.

The chemical exergy for the gaseous stream is calculated with the assumption that the gases behave as an ideal gas. Therefore, the gaseous chemical exergy ($\dot{E}_{ch,gas}$) can be calculated from equation 10 [47].

$$\dot{E}_{ch,gas} = \sum_i y_i \bar{E}^o{}_{chem,i} + R_o T_o \sum_i y_i log_e \left(\frac{\overline{f}_i}{f^o{}_i}\right) \quad (10)$$

where y_i and $\bar{E}^o{}_{chem,i}$ represent the mole fraction and molar chemical exergy of component *i*. R_o and T_o are the universal gas constant and the reference temperature (25 ^oC), respectively.

The physical exergy represents an expression of the thermomechanical usable exergy of the system. It is based on the enthalpy, entropy, and pressure. The physical exergy was computed based on equation 11 [47].

$$\bar{E}_{Phys} = (\overline{H} - \overline{H}_o) - T_o(\bar{S} - \bar{S}_o) \quad (11)$$

where $\overline{H}$ and $\bar{S}$ are the system enthalpy and entropy at a given temperature and pressure. In contrast, $\overline{H_o}$ and $\overline{S_o}$ represents the values of enthalpy and entropy at the environmental conditions.

4 Results and discussions

4.1 Mass and energy flow

The overall mass flow of the proposed methane pyrolysis unit is presented in Figure 5. The mass balance is used to evaluate the flow of mass in and out of the system, thereby promoting the practical design of the process. It should be mentioned that the mass balance results were expressed on a kg/hr basis with 100 kg/hr methane used as input feed. As illustrated in Figure 4, 76.8 % methane conversion is obtained at 800 ^{o}C and atmospheric pressure. However, increasing the temperature led to an elevation in methane conversion to 99.1% at 1000 ^{o}C. Regardless, lower temperature was selected because it is assumed that complete methane conversion can be attained under experimental conditions with a proper reactor design and a catalyst. Gaseous and solid carbon masses of 48.2 kg/hr and 74.5 kg/hr were produced per 100 kg/hr of methane field. The produced gases comprise 51% hydrogen and 49 % methane.

It is assumed that all the carbon produced from methane pyrolysis is combustible. In this case, it corresponds to 74.5kg/hr of carbon per 100 kg/hr of pure methane feed consumed. However, the combustion characteristics of the produced carbon would be one of the focuses of future experimental work. The solid char is combusted to produce the heat for the autothermal methane pyrolysis unit. Combustion of solid carbon produces different gases, including CO, CO_2, CH_4, and H_2. About 98% of the CH_4 produced during solid carbon combustion is removed via a CH_4 separation unit and sent to the combustion unit. Methane combustion yields about 138.6 kg/hr CO_2 and 12.7 kg/hr H_2. The methane combustion unit provides additional heat for the pyrolysis unit. The gaseous product from the CH_4 combustion unit is sent to the biomethanation unit, were about 22.7 kg/hr of CH_4 is produced and recycled as feed.

The energy balance of the proposed conceptual design is also presented in Figure 4. The energy needs of the process are determined as heat and energy requirements in addition to the energy provided by the feedstock and reaction products. The process is designed as an autothermal

system that does not require external heat. Therefore, an effective heat integration system is designed to promote the autothermal system. As shown in Figure 4, 67% of the energy in the methane feed is recovered by the produced gases, while the remainder is used for char production.

The energy efficiency of the process was estimated based on the lower heating values of the feedstock. The methane pyrolysis process operating at atmospheric pressure and 800 ^{o}C has an energy efficiency of 59.9%. Considering 90% combustion efficiency and 80% char gasification efficiency in the combustion chamber. The process is energy sufficient because enough product gas is recovered from the separation unit. In addition, applying an effective heat integration scheme helped lower the energy demand by 40.5%.

4.2 Exergy analysis

The overall exergy of destruction in the proposed mobile pyrolysis unit includes losses from heat exchangers, reactors, char separation unit, gasification system, and biomethanation unit. Details of the exergy loss in each processing unit are presented in Figure 6.

As shown in Figure 6a, the heat exchanger and the methane pyrolysis unit had the highest exergy of destruction. The heat exchanger and reactor accounted for 29% and 27% of the total exergy of destruction, respectively (figure 6b). During methane pyrolysis, solid carbon and hydrogen are produced via high-temperature methane decomposition without water and oxygen. The high-temperature decomposition leads to an increase in the exergy of destruction. Moreover, higher heating requirements from ambient to temperatures above 1000 ^{o}C could also be responsible for the elevation in the exergy of destruction from the heat exchangers. It should be mentioned that heat exchangers destroy exergy due to the transfer of heat across a specific temperature difference. Therefore, the exergy of destruction in heat exchangers is elevated at a higher temperature difference.

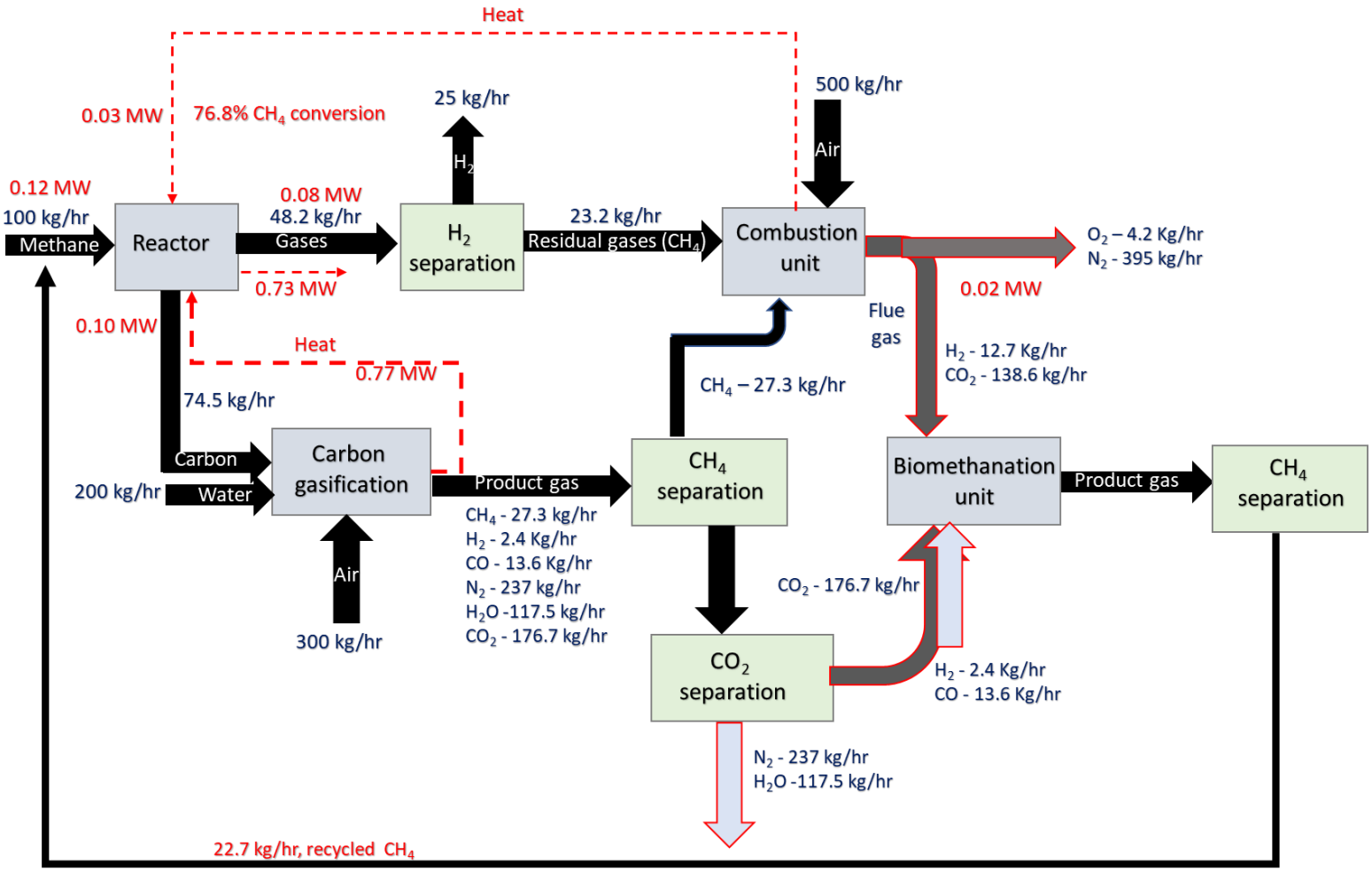

Figure **5:** Overall mass balance and energy flow for the proposed conceptual design of an autothermal mobile pyrolysis unit (results generated from Aspen Plus simulation). Note that the mass balance results presented are from the PFR at a reaction temperature of 800 ^{o}C. Although increasing temperature could elevate the CH_4 conversion, lower temperature was implemented because it is assumed that complete conversion could occur experimentally with efficient reactor design and a catalyst at similar temperatures.

The gasification and combustion unit also produced an increased exergy of the destruction of 36.1 kW and 40.5 kW, respectively. Both gasification and combustion units accounted for 15% and 17% of the total exergy of destruction, respectively (figure 6b). Char gasification consists of several intermediate reactions in which exergy is destroyed. These reactions include water-gas shift reactions, steam reforming, combustion, and Boudouard reactions [52]. Similarly, the combustion process consists of a reaction of methane with oxygen, as illustrated in equation 2. The reaction is highly exothermic; thus, energy accompanied by an exergy of destruction is released.

The exergy efficiency of the key processing unit is appraised and presented in Figure 7a. Since our study is a conceptual design and preliminary economic evaluation, it is important to determine the efficiency of each processing unit and anticipate the unit with future operational challenges. Exergy can also be used to compare the efficiency of different energy conversion technologies.

By knowing the exergy efficiency of a system or process, we can determine how efficiently it can perform the required task and identify ways to improve its efficiency. This can help to minimize the use of energy and save production costs. The combustion and biomethanation units have 98.4%, and 92.5% exergy efficiencies, respectively. In contrast, the exergy efficiencies of the methane pyrolysis and gasification unit are lower (48% and 43.1%, respectively). Although higher temperature favours hydrogen production and methane consumption, as shown in Figure 7b, the exergy efficiency of the methane pyrolysis reactor could also increase at the optimum temperature.

The findings reported herein are similar to those of the previous study in the literature [53]. With an increase in reactor temperature, an elevation in exergy efficiency was observed for the hydrothermal gasification process [53]. Our recent study also showed that the exergy efficiency

of an endothermic process is optimum at elevated temperatures [54]. In another study, Simpson et al. demonstrated the effectiveness of temperature in increasing the exergy efficiencies of an endothermic process [55]. Based on the exergy analysis results, it can be deduced that effective heat exchanger optimization is required to minimize the exergy loss in the heat exchangers and combustion unit. Also, it is desirable to reduce the reaction temperature to minimize the exergy of destruction in the pyrolysis reactor.

4.3 Economic analysis

An overall breakdown of the equipment purchase cost is presented in Figure 8. The cost of the methane pyrolysis reactor unit accounts for almost 28% of the EPC. Similarly, the flash separators and other auxiliary units such as heat exchangers, solid separators, and compressors account for 13%, 10%, and 8%, respectively. Methane pyrolysis reactions are carried out at significantly high temperatures and ambient pressures. Therefore, choosing a reactor material that could withstand such extreme temperatures is essential. In this case, a reactor material that can withstand harsh conditions with less susceptibility to corrosion is chosen, and the cost is used in the EPC appraisal. Inconel material is relatively expensive, and it is an excellent corrosion resistance compared to stainless steel [41]. Moreover, Inconel or stainless steel can withstand high temperatures when the refractory is made of ceramic insulation. The EPC was appraised based on the assumption that the reactor's construction material is made with Inconel. Microwave plasma reactors are usually made from stainless steel or Inconel. The quartz tube inside the microwave torch (not the entire reactor) prevents the flow of reactants via the waveguide to the magnetron because reactant injection is always perpendicular to the microwave energy. Heat exchangers are required for effective heat integration and recovery because the process is autothermal. Therefore, a combination of heat exchangers for heat integration could be responsible for the increased EPC cost relative to a process without effective heat integration.

Table 2 provides details of the economic analysis results. It should be mentioned that the CapEx and OpEx calculations have been meticulously described in the supplementary materials (Table S1 and S2). Since a mobile pyrolysis plant is considered in this work, the equipment purchase cost is lower than the typical equivalent cost for a stationary industrial plant. Furthermore, the cost of hydrogen transportation was not considered, and accompanying land costs were ignored – indicating the mobility of the proposed design (Tables S1 & S2 of the supplementary information). The CapEx and OpEx for the mobile pyrolysis unit are reported as 21.82 M.U.S.$ and 6 M.U.S.$, respectively. It should be noted that the fixed capital investment, which comprises direct and indirect costs, contributes significantly towards the CapEx. Similarly, the cost of feedstock and utilities are significant components of the OpEx.

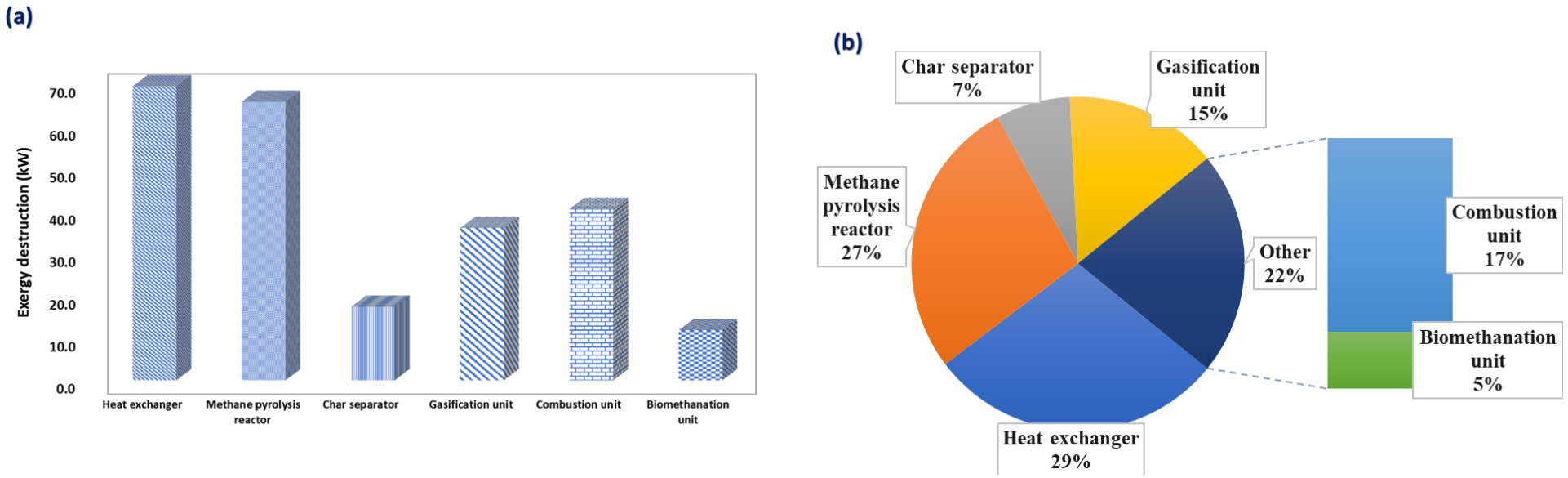

Figure 6 (a) An overview of the exergy of destruction for each processing unit in the proposed mobile pyrolysis unit (b) Percentage contribution of each processing unit to the total exergy of destruction

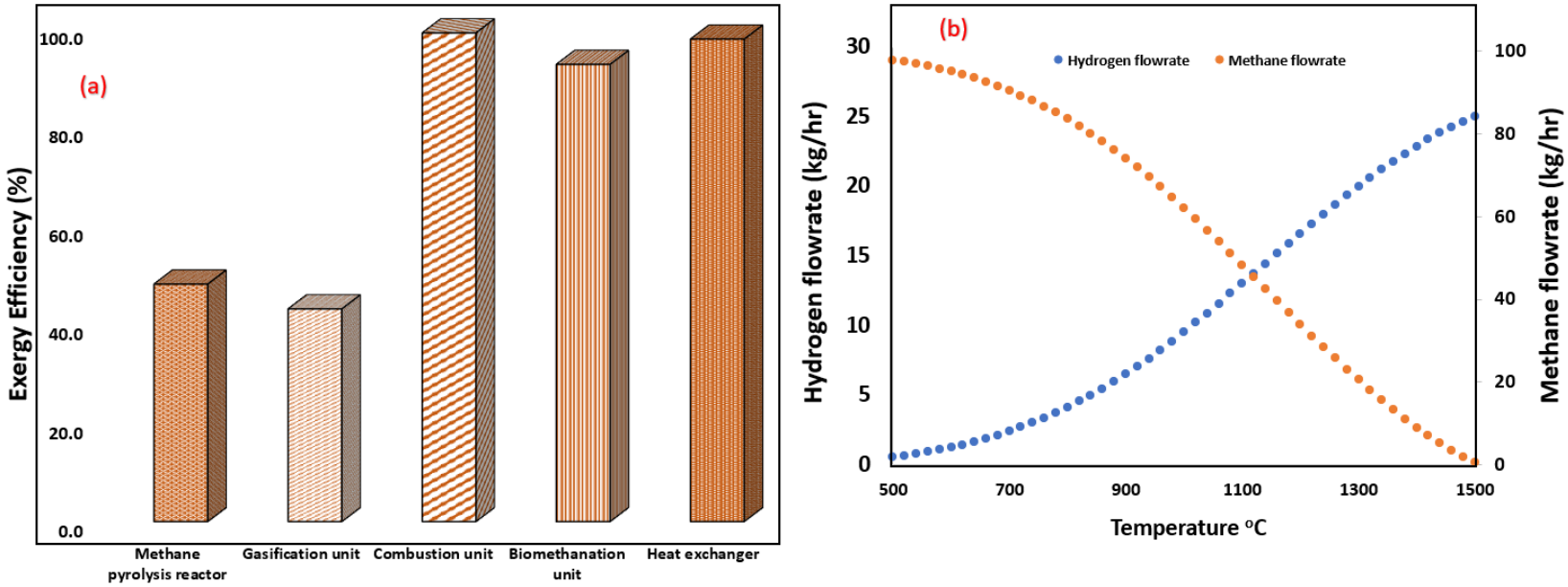

Figure 7(a) Comparative evaluation of the exergy efficiencies between different processing units. (b) Parametric effects of temperature on the hydrogen and methane flow rate at ambient pressure.

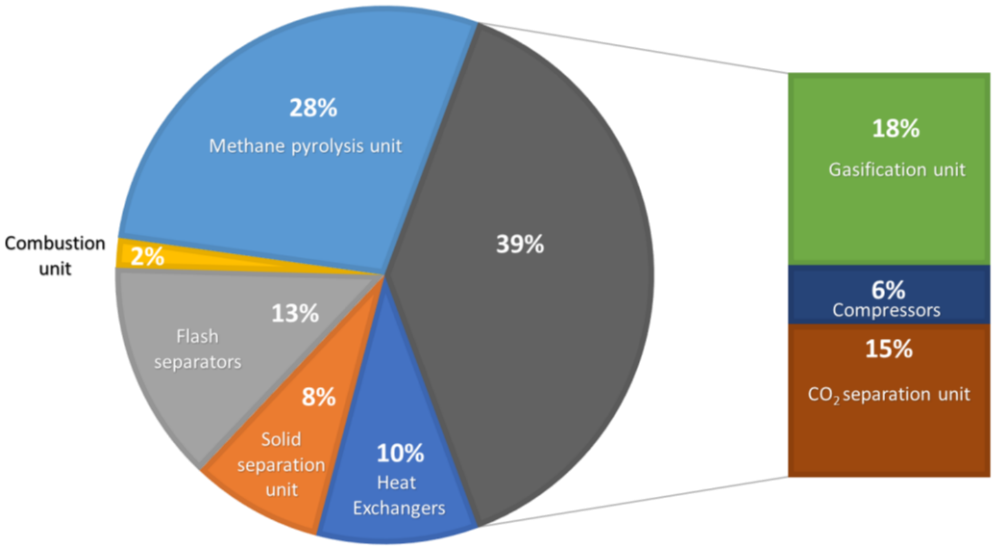

Figure 8: Breakdown of the overall cost of equipment purchase, including the installation cost.

Table 2: Summary of the economic analysis results.

Cost components	**Cost**	**Unit**
Equipment purchase cost (EPC)	6.16	M.U.S.$
Working capital (WC)	2.73	M.U.S.$
Fixed capital investment (FCI)	18.19	M.U.S.$
Capital expenditure (CAPEX)	21.82	M.U.S.$
Fixed operating cost (FOC)	1.73	M.U.S.$/y
Utility cost	0.16	M.U.S.$/y
Raw material cost (RMC)	4.12	M.U.S.$/y
Operating expenditure (OPEX)	6.00	M.U.S.$/y
Net present value	3.76	M.U.S.$
Return on investment (ROI)	45.57	%
Levelized cost of hydrogen (LCOH)	1.30	U.S.$/kg

The NPV, which describes the sum of the present values of all cash flow, including the initial investment, is estimated at 3.76 M.U.S.$. A positive NPV further highlights the profitability of the mobile pyrolysis unit.

The ROI is a very useful economic indicator that can be used to assess the efficiency and profitability of an investment. Compared to NPV, the ROI does not account for the time value of money. In the present study, the ROI was reported as 45.57%. Compared to the previous study on an industrial plant for hydrogen production, the capital expenditure of the proposed mobile pyrolysis unit is lower. A previous study reported a capital expenditure of M.U.S.$ 64.4 for a plant producing 200 kta of hydrogen from 800 kta of methane via methane pyrolysis in molten metal [56].

The LCOH of the autothermal methane pyrolysis unit obtained in this study is 1.30 U.S.$/kg. The price is significantly lower than LCOH from other hydrogen production routes, as illustrated in Table 3. Although all the articles cited in Table 3 adopted different cost estimation approaches and the price mentioned is mainly associated with the publication date, the cost still provides a reasonable comparison basis. Lower LCOH for the autothermal mobile methane pyrolysis unit proposed in this study further indicates that the unit is profitable. Coupling steam reforming of methane derived from natural gas with CO_2 capture remains the most economically competitive hydrogen production route with LCOH of 0.8 U.S.$/kg. If the process were performed without CO_2 capture, the LCOH would increase to a range of 1.88 – 2 U.S.$/kg [57,58]. Sorption-enhanced reforming of biomass showed a relatively high LCOH of 10.93 – 11 U.S.$/kg compared to other processes [59]. Although the sorption-enhanced reforming gasification process produces a nitrogen-free, high calorific product gas containing hydrogen, the use of limestone as bed material, in situ CO_2 capture, and the high reaction temperature is a major reason for the increased process economics. The LCOH produced from other energy-intensive methods, such as electrolysis, is higher due to the energy requirement of the process in the form of electricity.

Table 3: Comparative evaluation of the LCOH for different production processes.

Hydrogen production process	**LCOH/Minimum selling price (U.S.$/kg)**	**Ref.**
Autothermal mobile methane pyrolysis unit	1.3	This work
Methane steam reforming with carbon capture	0.8	Acar and Dincer [58]
Methane steam reforming without carbon capture	1.88-2	Al-Qahtani et al. [57]
Sorption-enhanced reforming biomass gasification	10.93-11	Schweitzer et al. [59]
Fluidized bed gasification	3.1-4.0	Salkuyeh et al. [60]
SCWG integrated with CO_2 removal unit and energy self-sufficient	1.94-1.97	Okolie et al. [41].
Dark fermentation	2.6	Salkuyeh et al. (2018)
Coal gasification with CO_2 sequestration	0.9-1.7	Acar and Dincer [58]
Water-driven electrolysis with solar energy	2.89	Yates et al. [61]
Pyrolysis	1-2	Acar and Dincer [58]
Coal gasification	0.8-1.3	Acar and Dincer [58]

4.4 Sensitivity analysis

The economic metrics such as the LCOH and NPV are impacted by several parameters such as cost of feedstock, labour cost, EPC, and tax rate. The impact of these parameters on the NPV and LCOH is presented in Figure 9. The sensitivity analysis appraises the impact of varying these parameters at ± 20% on the economic metrics. The tax rate, EPC, and feedstock cost had the greatest impact on the NPV. With a 20% decrease in feedstock cost, the NPV rose from 3.76 M.U.S.$ to 4.35 M.U.S.$. Similarly, a decline in tax rate led to an increase in NPV up to

4.09 M.U.S.$. In contrast, a 20% increase in the feedstock cost and tax rate led to a decline in NPV to 3.2 M.U.S.% and 3.44 M.U.S.$, respectively.

A change in the tax rate does not impact the LCOH. Similarly, the labour and utility cost change had a significantly lower impact on the NPV and LCOH. For instance, Figure 9b shows that a 20% increase in utility cost only produced an NPV value of 3.74 M.U.S.$ and an LCOH value of 1.31 U.S.$/kg.

Other factors, such as EPC and feedstock cost, significantly influenced the LCOH. The feedstock used in the present study includes pure methane, compressed air, and water. However, the cost of pure methane is dependent on the logistics and purification costs. H_2S gas is naturally present in natural gas and requires a higher separation cost to recover pure methane. This could potentially influence the feedstock cost. The utility cost had little impact on the LCOH due to the improved energy integration adopted in the proposed technology. In addition, the introduction of gasification and combustion units to supply heat requirements further minimizes the utility cost.

4.5 Key issues of the proposed technology and study limitations

The present study proposes a conceptual design that produces hydrogen through catalytic methane pyrolysis as well as the produced carbon gasification. Although the economic analysis indicates that the process is profitable based on positive NPV and lower LCOH, the profitability of the process could also be directly attributed to heat integration via char gasification. Regardless, there are several study limitations.

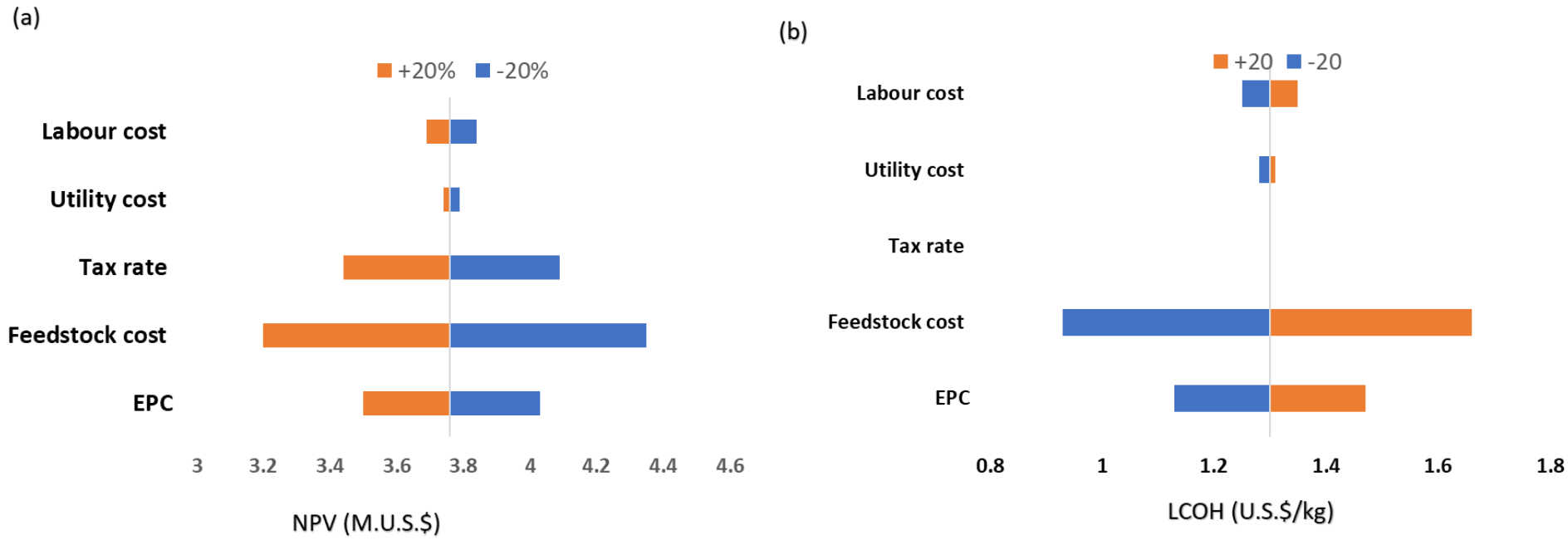

Figure 9: Sensitivity analysis demonstrating the impact of different parameters on the (a) NPV (b) LCOH

The methane used in the study is pure methane. In reality, natural gas comprises several mixtures of gases, including saturated light paraffin such as methane and ethane and non-hydrocarbon gases. Combustible and non-combustible gases such as nitrogen, carbon dioxide, hydrogen sulphide, and noble gases are often separated before the pyrolysis reaction. Recovery of pure methane from natural gas requires processing steps such as gas sweetening and dehydration. These steps are not accounted for in the process simulation. Although, they are clearly defined in the economic model via the feedstock cost.

Another limitation is the quality and quantity of carbon products from methane pyrolysis. It was assumed that all the produced carbon is combustible and sufficient to generate the heat requirements for the process. While this is not always the case, future studies would focus on experimental verification, analytical characterization of the carbon product to determine its combustion characteristics and detailed heat integration.

This study has not accounted for tax exemption, carbon credits, and biofuel subsidy incentives implemented by several studies. The inclusion of these government incentives could lower the LCOH presented in the study. However, it should be mentioned that these incentives vary for different countries and are highly unpredictable. Therefore, it is very difficult to implement them in the economic model.

The project's scope did not extend to prototyping or a full-scale demonstration of the mobile pyrolysis unit. Therefore, the experimental data is currently unavailable. Although, plans for developing a prototype and full-scale demonstration are currently in progress. However, the simulation results have been verified against published experimental data and are presented in the study. The authors are aware that there is a risk of projecting performance information to full scale in the absence of experimental data. Regardless, the model validation presented herein could help answer certain technical questions and to generate baseline performance

data. The novel reactor design integrating a microwave-based plasma torch integrated with a multi-layered liquid metal bubble column reactor is a new concept that has not been experimentally verified. There could be some challenges during experimental verification which would be the scope of future studies. Such design could suffer from issues such as energy efficiency and optimization of product recovery.

Future studies would also focus on a comprehensive energy and exergy analysis of each processing unit. The relationship between exergy efficiency and efficiency metrics such as energy efficiency, conversion efficiency, product selectivity, and yield are targeted scope of future studies. A comprehensive cradle-to-grave lifecycle assessment is also proposed to appraise the environmental impact of the proposed technology. However, these studies could only be performed adequately when data from a demonstration plant is available.

Process simulation results shows complete conversion at higher temperatures greater than 1000 ^{o}C. However, a temperature of 800 ^{o}C was implemented during economic evaluation. This is due to the assumptions that the use of a catalysts and efficient reactor design implemented in this study would lead to a complete conversion of methane at 800 ^{o}C or lower temperature.

5 Conclusion

This study presents for the first time the conceptual design of a mobile autothermal plasma methane pyrolysis unit for onsite hydrogen production. Energy, exergy, and techno-economic analysis were investigated to evaluate the efficiency and performance of the entire process. The stochastic method based on Monte Carlo simulation was used to evaluate the techno-economic analysis and sensitivity analysis of the conceptual design by quantifying the uncertainty and associated risk of the process. The following key results were reported from the mobile demonstration unit.

- The process is profitable, with a positive net present value (NPV) ranging from 3.76 – 4.35 M.U.S.$. and a lower levelized cost of hydrogen range of 1.3 – 1.47 U.S.$/kg.
- The return on investment (ROI) was reported as 45.57%. Compared to the previous study on an industrial plant for hydrogen production, the capital expenditure of the proposed mobile pyrolysis unit is lower.
- Although there is no available experimental data for model validation, a comparison of the model results with studies on plasma pyrolysis shows similar methane conversion with a deviation of less than 2%.
- From the sensitivity analysis, the tax rate, EPC, and feedstock cost were found to have a significant effect on the NPV. In contrast, labor and utility costs had a less significant impact on the NPV and levelized cost of hydrogen.

In summary, this study has demonstrated that a mobile autothermal plasma pyrolysis unit for onsite hydrogen production will be useful for the future process development of mobile biomass pyrolysis systems, especially in North America, and the implementation of sustainable technologies.

Acknowledgement

The authors would like to thank the Editor and Reviewers. Their comments and suggestions helped improved the quality of the study.

References

[1] Kerscher F, Stary A, Gleis S, Ulrich A, Klein H, Spliethoff H. Low-carbon hydrogen production via electron beam plasma methane pyrolysis: Techno-economic analysis and carbon footprint assessment. Int J Hydrogen Energy 2021;46:19897–912. https://doi.org/10.1016/j.ijhydene.2021.03.114.

[2] Epelle EI, Desongu KS, Obande W, Adeleke AA, Ikubanni PP, Okolie JA, et al. A comprehensive review of hydrogen production and storage: A focus on the role of nanomaterials. Int J Hydrogen Energy 2022;47:20398–431. https://doi.org/10.1016/j.ijhydene.2022.04.227.

[3] van der Spek M, Banet C, Bauer C, Gabrielli P, Goldthorpe W, Mazzotti M, et al. Perspective on the hydrogen economy as a pathway to reach net-zero CO2 emissions in Europe†. Energy Environ Sci 2022;15:1034–77. https://doi.org/10.1039/d1ee02118d.

[4] Tollefson J. COVID curbed carbon emissions in 2020 - but not by much. Nature 2021;589:343. https://doi.org/10.1038/d41586-021-00090-3.

[5] Parfenov VE, Nikitchenko N V., Pimenov AA, Kuz'min AE, Kulikova M V., Chupichev OB, et al. Methane Pyrolysis for Hydrogen Production: Specific Features of Using Molten Metals. Russian Journal of Applied Chemistry 2020;93:625–32. https://doi.org/10.1134/S1070427220050018.

[6] Sánchez-Bastardo N, Schlögl R, Ruland H. Response to Comment on "Methane Pyrolysis for Zero-Emission Hydrogen Production: A Potential Bridge Technology from Fossil Fuels to a Renewable and Sustainable Hydrogen Economy." Ind Eng Chem Res 2021;60:17795–6. https://doi.org/10.1021/acs.iecr.1c04435.

[7] Gunes B. A critical review on biofilm-based reactor systems for enhanced syngas fermentation processes. Renewable and Sustainable Energy Reviews 2021;143:110950. https://doi.org/10.1016/j.rser.2021.110950.

[8] Sánchez-Bastardo N, Schlögl R, Ruland H. Methane Pyrolysis for CO2-Free H2 Production: A Green Process to Overcome Renewable Energies Unsteadiness. Chem Ing Tech 2020;92:1596–609. https://doi.org/10.1002/cite.202000029.

[9] Dagle RA, Dagle V, Bearden MD, Holladay JD, Krause TR, Ahmed S. An Overview of Natural Gas Conversion Technologies for Co-Production of Hydrogen and Value-Added Solid Carbon Products. (No PNNL-26726; ANL-17/11) Pacific Northwest National Lab(PNNL), Richland, WA (United States); Argonne National Lab(ANL), Argonne, IL (United States) 2017:65. https://doi.org/10.2172/1411934.

[10] Muradov N, Smith F, Bockerman G, Scammon K. Thermocatalytic decomposition of natural gas over plasma-generated carbon aerosols for sustainable production of hydrogen and carbon. Appl Catal A Gen 2009;365:292–300. https://doi.org/10.1016/j.apcata.2009.06.031.

[11] Akande O, Lee BJ. Plasma steam methane reforming (PSMR) using a microwave torch for commercial-scale distributed hydrogen production. Int J Hydrogen Energy 2022;47:2874–84. https://doi.org/10.1016/j.ijhydene.2021.10.258.

[12] Mašláni A, Hrabovský M, Křenek P, Hlína M, Raman S, Sikarwar VS, et al. Pyrolysis of methane via thermal steam plasma for the production of hydrogen and carbon black. Int J Hydrogen Energy 2021;46:1605–14. https://doi.org/10.1016/j.ijhydene.2020.10.105.

[13] Parkinson B, Matthews JW, McConnaughy TB, Upham DC, McFarland EW. Techno-Economic Analysis of Methane Pyrolysis in Molten Metals: Decarbonizing Natural Gas. Chem Eng Technol 2017;40:1022–30. https://doi.org/10.1002/ceat.201600414.

[14] Dors M, Nowakowska H, Jasiński M, Mizeraczyk J. Chemical kinetics of methane pyrolysis in microwave plasma at atmospheric pressure. Plasma Chemistry and Plasma Processing 2014;34:313–26. https://doi.org/10.1007/s11090-013-9510-4.

[15] Marquardt T, Bode A, Kabelac S. Hydrogen production by methane decomposition: Analysis of thermodynamic carbon properties and process evaluation. Energy Convers Manag 2020;221:113125. https://doi.org/10.1016/J.ENCONMAN.2020.113125.

[16] Pruvost F, Cloete S, Arnaiz del Pozo C, Zaabout A. Blue, green, and turquoise pathways for minimizing hydrogen production costs from steam methane reforming with CO2 capture. Energy Convers Manag 2022;274:116458. https://doi.org/10.1016/J.ENCONMAN.2022.116458.

[17] Keuchel F, Raveendran T, Agar DW. Simulation of chlorine-mediated autothermal methane pyrolysis for hydrogen production. Int J Hydrogen Energy 2022. https://doi.org/10.1016/J.IJHYDENE.2022.10.122.

[18] Raja RB, Sarathi R, Vinu R. Selective Production of Hydrogen and Solid Carbon via Methane Pyrolysis Using a Swirl-Induced Point–Plane Non-thermal Plasma Reactor. Energy and Fuels 2022;36:826–36. https://doi.org/10.1021/acs.energyfuels.1c03383.

[19] Heijkers S, Aghaei M, Bogaerts A. Plasma-Based CH4 Conversion into Higher Hydrocarbons and H2: Modeling to Reveal the Reaction Mechanisms of Different Plasma Sources. Journal of Physical Chemistry C 2020;124:7016–30. https://doi.org/10.1021/acs.jpcc.0c00082.

[20] Parmar KR, Pant KK, Roy S. Blue hydrogen and carbon nanotube production via direct catalytic decomposition of methane in fluidized bed reactor: Capture and extraction of carbon in the form of CNTs. Energy Convers Manag 2021;232:113893. https://doi.org/10.1016/J.ENCONMAN.2021.113893.

[21] Barati Dalenjan M, Rashidi A, Khorasheh F, Ardjmand M. Effect of Ni ratio on mesoporous Ni/MgO nanocatalyst synthesized by one-step hydrothermal method for thermal catalytic decomposition of CH4 to H2. Int J Hydrogen Energy 2022;47:11539–51. https://doi.org/10.1016/J.IJHYDENE.2022.01.185.

[22] Noh YG, Lee YJ, Kim J, Kim YK, Ha JS, Kalanur SS, et al. Enhanced efficiency in CO2-free hydrogen production from methane in a molten liquid alloy bubble column reactor with zirconia beads. Chemical Engineering Journal 2022;428:131095. https://doi.org/10.1016/J.CEJ.2021.131095.

[23] Reddy SN, Nanda S, Kozinski JA. Supercritical water gasification of glycerol and methanol mixtures as model waste residues from biodiesel refinery. Chemical Engineering Research and Design 2016;113:17–27. https://doi.org/10.1016/j.cherd.2016.07.005.

[24] Adamu S, Binous H, Razzak SA, Hossain MM. Enhancement of glucose gasification by Ni/La 2 O 3 -Al 2 O 3 towards the thermodynamic extremum at supercritical water conditions. Renew Energy 2017;111:399–409. https://doi.org/10.1016/j.renene.2017.04.020.

[25] Nikoo MK, Saeidi S, Lohi A. A comparative thermodynamic analysis and experimental studies on hydrogen synthesis by supercritical water gasification of glucose. Clean Technol Environ Policy 2015;17:2267–88. https://doi.org/10.1007/s10098-015-0965-2.

[26] Barbier J, Charon N, Dupassieux N, Loppinet-Serani A, Mahé L, Ponthus J, et al. Hydrothermal conversion of glucose in a batch reactor. A detailed study of an experimental key-parameter: The heating time. Journal of Supercritical Fluids 2011;58:114–20. https://doi.org/10.1016/j.supflu.2011.05.004.

[27] Louw J, Schwarz CE, Burger AJ. Catalytic supercritical water gasification of primary paper sludge using a homogeneous and heterogeneous catalyst: Experimental vs. thermodynamic equilibrium results. Bioresour Technol 2016;201:111–20. https://doi.org/10.1016/j.biortech.2015.11.043.

[28] HYSEP. Hydrogen Separation Module Type Hysep® 108 – Hysep. 2022 n.d. https://www.hysep.com/products/hysep-108/ (accessed December 27, 2022).

[29] Marcantonio V, de Falco M, Capocelli M, Bocci E, Colantoni A, Villarini M. Process analysis of hydrogen production from biomass gasification in fluidized bed reactor with different separation systems. Int J Hydrogen Energy 2019;44:10350–60. https://doi.org/10.1016/J.IJHYDENE.2019.02.121.

[30] Zhou R, Pan Y, Xing W, Xu N. Advanced microporous membranes for H2/CH4 separation: Challenges and perspectives. Advanced Membranes 2021;1:100011. https://doi.org/10.1016/J.ADVMEM.2021.100011.

[31] Brady PD. An Economic Analysis of Mobile Pyrolysis for Northern New Mexico Forests - Google Search. 2011.

[32] Reading truck. Calculating Your ~~Truck’' 's~~ Truck's Maximum Payload and Towing Capacity 2022. https://www.readingtruck.com/calculating-your-trucks-maximum-payload-and-towing-capacity/ (accessed December 28, 2022).

[33] Boo J, Ko EH, Park NK, Ryu C, Kim YH, Park J, et al. Methane Pyrolysis in Molten Potassium Chloride: An Experimental and Economic Analysis. Energies 2021, Vol 14, Page 8182 2021;14:8182. https://doi.org/10.3390/EN14238182.

[34] Upham DC, Agarwal V, Khechfe A, Snodgrass ZR, Gordon MJ, Metiu H, et al. Catalytic molten metals for the direct conversion of methane to hydrogen and separable carbon. Science (1979) 2017;358:917–21. https://doi.org/10.1126/SCIENCE.AAO5023/SUPPL_FILE/AAO5023S2.MP4.

[35] Parkinson B, Tabatabaei M, Upham DC, Ballinger B, Greig C, Smart S, et al. Hydrogen production using methane: Techno-economics of decarbonizing fuels and chemicals. Int J Hydrogen Energy 2018;43:2540–55. https://doi.org/10.1016/J.IJHYDENE.2017.12.081.

[36] Ando T, Ueno K, Taniguchi S, Takagi T. Induction pump for high-temperature molten metals using rotating twisted magnetic field: Thrust measurement experiment with solid conductors. IEEE Trans Magn 2002;38:1789–96. https://doi.org/10.1109/TMAG.2002.1017772.

[37] Mason S, Cameron P, Curtis A. Port Augusta Solar Thermal Generation Feasibility Study Stage 1-Pre-feasibility Study Options Study Report Client: Alinta Energy Title: Port Augusta Solar Thermal Generation Feasibility Study Stage 1-Pre-feasibility Study Subtitle: Options Study Report Contents 2014.

[38] Jasiński M, Czylkowski D, Hrycak B, Dors M, Mizeraczyk J. Atmospheric pressure microwave plasma source for hydrogen production. Int J Hydrogen Energy 2013;38:11473–83. https://doi.org/10.1016/J.IJHYDENE.2013.05.105.

[39] Fulcheri L, Rohani V-J, Wyse E, Hardman N, Dames E. An energy-efficient plasma methane pyrolysis process for high yields of carbon black and hydrogen. Int J Hydrogen Energy 2022. https://doi.org/10.1016/J.IJHYDENE.2022.10.144.

[40] Turton R, Bailie R, Whiting W, Shaeiwitz J. Analysis, synthesis, and design of chemical processes. vol. 36. 2009. https://doi.org/10.5860/choice.36-0974.

[41] Okolie JA, Nanda S, Dalai AK, Kozinski JA. Techno-economic evaluation and sensitivity analysis of a conceptual design for supercritical water gasification of soybean straw to produce hydrogen. Bioresour Technol 2021;331:125005. https://doi.org/10.1016/j.biortech.2021.125005.

[42] Zimmermann AW, Wunderlich J, Müller L, Buchner GA, Marxen A, Michailos S, et al. Techno-Economic Assessment Guidelines for CO2 Utilization. Front Energy Res 2020;0:5. https://doi.org/10.3389/FENRG.2020.00005.

[43] Sahoo K, Bilek E, Bergman R, Mani S. Techno-economic analysis of producing solid biofuels and biochar from forest residues using portable systems. Appl Energy 2019;235:578–90. https://doi.org/10.1016/J.APENERGY.2018.10.076.

[44] Gutiérrez Ortiz FJ. Techno-economic assessment of supercritical processes for biofuel production. J Supercrit Fluids 2020;160:104788. https://doi.org/10.1016/J.SUPFLU.2020.104788.

[45] Minutillo M, Perna A, Forcina A, di Micco S, Jannelli E. Analyzing the levelized cost of hydrogen in refueling stations with ~~on-site~~ onsite hydrogen production via water electrolysis in the Italian scenario. Int J Hydrogen Energy 2021;46:13667–77. https://doi.org/10.1016/J.IJHYDENE.2020.11.110.

[46] Zhao X, Yao G, Tyner WE. Quantifying breakeven price distributions in stochastic techno-economic analysis. Appl Energy 2016;183:318–26. https://doi.org/10.1016/j.apenergy.2016.08.184.

[47] Umenweke GC, Pace RB, Santillan-Jimenez E, Okolie JA. Techno-economic and life-cycle analyses of sustainable aviation fuel production via integrated catalytic deoxygenation and hydrothermal gasification. Chemical Engineering Journal 2023;452:139215. https://doi.org/10.1016/J.CEJ.2022.139215.

[48] Michailos S, Parker D, Webb C. Design, Sustainability Analysis and Multiobjective Optimisation of Ethanol Production via Syngas Fermentation. Waste Biomass Valorization 2019;10:865–76. https://doi.org/10.1007/S12649-017-0151-3/FIGURES/8.

[49] Rahbari A, Venkataraman MB, Pye J. Energy and exergy analysis of concentrated solar supercritical water gasification of algal biomass. Appl Energy 2018;228:1669–82. https://doi.org/10.1016/j.apenergy.2018.07.002.

[50] Atienza-Martínez M, Ábrego J, Mastral JF, Ceamanos J, Gea G. Energy and exergy analyses of sewage sludge thermochemical treatment. Energy 2018;144:723–35. https://doi.org/10.1016/J.ENERGY.2017.12.007.

[51] Kaushik SC, Singh OK. Estimation of chemical exergy of solid, liquid, and gaseous fuels used in thermal power plants. J Therm Anal Calorim 2014;115:903–8. https://doi.org/10.1007/S10973-013-3323-9/FIGURES/3.

[52] Prins MJ, Ptasinski KJ, Janssen FJJG. Thermodynamics of gas-char reactions: first and second law analysis. Chem Eng Sci 2003;58:1003–11. https://doi.org/10.1016/S0009-2509(02)00641-3.

[53] Rahbari A, Venkataraman MB, Pye J. Energy and exergy analysis of concentrated solar supercritical water gasification of algal biomass. Appl Energy 2018;228:1669–82. https://doi.org/10.1016/J.APENERGY.2018.07.002.

[54] Umenweke GC, Pace RB, Santillan-Jimenez E, Okolie JA. Techno-economic and life-cycle analyses of sustainable aviation fuel production via integrated catalytic deoxygenation and hydrothermal gasification. Chemical Engineering Journal 2023;452:139215. https://doi.org/10.1016/J.CEJ.2022.139215.

[55] Simpson AP, Lutz AE. Exergy analysis of hydrogen production via steam methane reforming. Int J Hydrogen Energy 2007;32:4811–20. https://doi.org/10.1016/J.IJHYDENE.2007.08.025.

[56] Parkinson B, Matthews JW, McConnaughy TB, Upham DC, McFarland EW. Techno-Economic Analysis of Methane Pyrolysis in Molten Metals: Decarbonizing Natural Gas. Chem Eng Technol 2017;40:1022–30. https://doi.org/10.1002/CEAT.201600414.

[57] Al-Qahtani A, Parkinson B, Hellgardt K, Shah N, Guillen-Gosalbez G. Uncovering the true cost of hydrogen production routes using life cycle monetisation. Appl Energy 2021;281:115958. https://doi.org/10.1016/J.APENERGY.2020.115958.

[58] Acar C, Dincer I. Review and evaluation of hydrogen production options for better environment. J Clean Prod 2019;218:835–49. https://doi.org/10.1016/J.JCLEPRO.2019.02.046.

[59] Schweitzer D, Albrecht FG, Schmid M, Beirow M, Spörl R, Dietrich RU, et al. Process simulation and techno-economic assessment of SER steam gasification for hydrogen production. Int J Hydrogen Energy 2018;43:569–79. https://doi.org/10.1016/J.IJHYDENE.2017.11.001.

[60] Salkuyeh YK, Saville BA, MacLean HL. Techno-economic analysis and life cycle assessment of hydrogen production from different biomass gasification processes. Int J Hydrogen Energy 2018;43:9514–28. https://doi.org/10.1016/J.IJHYDENE.2018.04.024.

[61] Yates J, Daiyan R, Patterson R, Egan R, Amal R, Ho-Baille A, et al. Techno-economic Analysis of Hydrogen Electrolysis from Off-Grid Stand-Alone Photovoltaics Incorporating Uncertainty Analysis. Cell Rep Phys Sci 2020;1:100209. https://doi.org/10.1016/J.XCRP.2020.100209.